Mechanistic model of multi-frequency complex conductivity of porous media containing water-wet nonconductive and conductive particles at various water saturations

Yuteng Jin, Siddharth Misra, Dean Homan, John Rasmus, André Revil

Advances in Water Resources 130 (2019) 244–257

Contents lists available at ScienceDirect

Advances in Water Resources

journal homepage: www.elsevier.com/locate/advwatres

Mechanistic model of multi-frequency complex conductivity of porous media containing water-wet nonconductive and conductive particles at various water saturations

Yuteng Jin [a], Siddharth Misra [a,*], Dean Homan [b], John Rasmus [b], André Revil [c]

[a] Mewbourne College of Earth and Energy, University of Oklahoma, Norman, OK, USA
[b] Schlumberger Technology Corporation, Sugarland, TX, USA
[c] CNRS-ISTERRE, France

A B S T R A C T

Electrically conductive particles, such as pyrites, and surface-charge-bearing nonconductive particles, such as clays, are commonly present in water-bearing subsurface formations. Under an external electric field generated by electromagnetic measurement tool, these particles give rise to interfacial polarization (IFP) effects, which causes frequency dispersion of effective conductivity and effective permittivity of the mixture containing such particles. The neglect of IFP effects can lead to inaccurate estimation of petrophysical properties of formations, especially in clay- and pyrite- rich formations. In this paper, we developed a mechanistic model that couples surface-conductance-assisted interfacial polarization (SCAIP) model with perfectly polarized interfacial polarization (PPIP) model to estimate effective conductivity and effective permittivity of homogeneous formations containing both nonconductive and conductive particles at various fluids saturations. The model is developed based on the Poisson-Nernst-Planck (PNP) equations for a dilute solution in a weak electrical field regime to calculate the dipolarizability of the representative volume comprising a single isolated spherical particle in an electrolyte host. Then the effective medium theory is used to determine effective complex conductivity of the whole mixture. The result shows that the conductive particles dominate the frequency dispersion of complex conductivity due to IFP effects compared to nonconductive particles.

1. Introduction

Interfacial polarization phenomena (Dukhin et al., 1974; Wong, 1979; Schmuck and Bazant, 2015) influences the migration, accumulation, depletion, and diffusion of charge carriers. If neglected, interfacial polarization (IFP) effects will lead to inaccuracy when estimating petrophysical properties of formations using conventional resistivity/conductivity/permittivity interpretation methods (Clavier et al., 1976; Misra et al., 2016a; Zhao et al., 2016). Some of the interpretation techniques for the subsurface galvanic resistivity (laterolog), electromagnetic (EM) induction and EM dielectric dispersion logs do not consider the IFP effects (Anderson et al., 2007; Corley et al., 2010), which cause inaccurate estimates for pyrite-rich sedimentary rocks (Altman et al., 2008) and pyrite- and graphite-rich organic source rocks (Altman et al., 2008). Although in the last decade, some papers included IFP effect in EM induction logs (MacLennan et al., 2013), or in dielectric model which considers cation exchange capacity (Revil, 2013), there is still a need to investigate the IFP effect. Recently, for hydrocarbon volume estimation, Deng et al. (2018) applied spectral induced polarization method to estimate oil saturation in oil-contaminated clayey soils. Freed et al. (2018) also developed a physics-based model for the dielectric response that accounts for the IFP effect due to the cation exchange capacity in low-salinity shaly sands formations.

Mechanistic model of the IFP phenomena can improve resistivity/conductivity/permittivity interpretation in clay- and conductive-mineral-rich formations. To model the IFP effect of electrically conductive inclusions, Misra et al. (2016b) applied Poisson-Nernst-Planck (PNP) equation. Their model predictions have a good match with laboratory measurements on conductive-mineral-bearing mixtures. Moreover, several mathematical models have been developed in the fields of petrology (Revil et al., 2017), geophysics (Revil, 2012; Placencia-Gómez and Slater, 2014), biology (Grosse and Schwan, 1992; Zheng and Wei, 2011), electrochemistry (Chu and Bazant, 2006) and colloidal science (Grosse and Barchini, 1992; Grosse et al., 1998), all of which facilitate the study of interfacial polarization effects arising from various mechanisms.

In this paper, we develop a model that couples the interfacial polarization of uniformly distributed water-wet nonconductive spherical grains possessing surface conductance with interfacial polarization of uniformly distributed conductive spherical inclusions in redox-inactive conditions at various water saturations. The proposed model can be applied to estimate effective conductivity and effective permittivity of homogeneous formations containing both conductive and nonconductive particles at various fluids saturations.

* Corresponding author.
E-mail address: misra@ou.edu (S. Misra).

https://doi.org/10.1016/j.advwatres.2019.06.015
Received 4 February 2019; Received in revised form 25 June 2019; Accepted 27 June 2019
Available online 28 June 2019
0309-1708/Published by Elsevier Ltd.

Acronyms

EM	electromagnetic
IFP	interfacial polarization
PDE	partial differential equations
PNP	Poisson–Nernst–Planck
PPIP	perfectly polarized interfacial polarization
PS	PPIP-SCAIP
SCAIP	surface-conductance-assisted interfacial polarization

Symbols

a	characteristic length of inclusion phase (m)
c	charge density variation ($1/m^3$)
d	net charge density variation ($1/m^3$)
D	diffusion coefficient of charge carriers (m^2/s)
Δ (∇^2)	Laplace's operator
e	Euler's number
$\boldsymbol{e}$	electric field vector
E_0	amplitude of the electric field (V)
ε	dielectric permittivity (F/m)
ε_0	vacuum permittivity (8.854×10^{-12} F/m)
ε_{eff}	effective dielectric permittivity of the mixture (F/m)
ε_r	relative permittivity
f	frequency (Hz)
$f(\omega)$	dipolarizability (dipolar field coefficient)
i	square root of -1
i_n	modified spherical Bessel function of the first kind of nth order
I_n	modified Bessel function of the first kind of nth order
$\boldsymbol{j}$	current density (A/m^3)
k_B	Boltzmann's constant
k_n	modified spherical Bessel function of the second kind of nth order
K_n	modified Bessel function of the second kind of nth order
λ	surface conductance (S)
λ_D	Debye screening length (m)
μ	electrical mobility [$m^2/(V{\cdot}s)$]
n	an integer referring to the order of the standing wave solution
N	charge carrier density ($1/m^3$)
ω	angular frequency of the electric field (rad/s)
P_f	net free charge density (C/m^3)
P_n^0	associated Legendre functions of the first kind of nth order
φ	electrical potential (V)
ϕ	volume fraction (%)
q	elementary charge (1.6×10^{-19} C)
Q_n^0	associated Legendre functions of the second kind of nth order
r	radial distance along the normal to the interface (m)
ρ	surface charge density (C/m^2)
s	total ion density variation ($1/m^3$)
σ	electrical conductivity (S/m)
σ^*	complex electrical conductivity (S/m)
σ_{eff}	effective electrical conductivity of the mixture (S/m)
σ^*_{eff}	effective complex electrical conductivity of the mixture (S/m)
t	time (s)
T	absolute temperature (K)
θ	angle between the normal to the interface and the incident external electric field (°)
Z	charge number

Subscripts

0	at time equal to 0 s
c	clay
$cond$	conductive particles
eff	effective
h	host medium
i	inclusion phase
j	type of medium/phase
n	an integer referring to the order
$\hat{n}$	unit vector
$ncond$	nonconductive particles
o	oil
p	pyrite
r	relative
s	sand

Superscripts

+	positively charged carrier
−	negatively charged carrier

1.1. Interfacial polarization around surface-charge-bearing spherical nonconductive particles

Various mixing models have been developed to quantify the effects of various interfacial polarization phenomena. The model proposed by Schwarz (1962) considers interfacial polarization (IFP) effect around charged nonconductive particles. It assumes a diffusion of counterion layer moving along the surface of the charged particle by calculating the potential outside the counterion layer as a solution of Laplace's equation rather than Poisson's equation. However, this model fails to account for all the bulk diffusion effects. In contrast, Dukhin et al. (1974) concluded that the mechanism behind interfacial polarization is the diffusion of ions in the bulk electrolyte around the particle. They were unable to provide analytical expressions for IFP effects in terms of various relaxation parameters due to mathematical complexity caused by non-linearity of Dukhin et al. (1974) equation. This model, called the standard model in colloidal chemistry, does not consider the existence of a Stern layer with mobile ions. Grosse and Foster (1987) developed an analytical solution of IFP effect by developing a simplified model of charged nonconductive spherical particles in bulk electrolyte. In their model, positive ions from the bulk electrolyte can freely exchange with the positively charged counterion layer while the negative ions are excluded from the counterion layer. This model was generalized in Grosse (1988) by allowing arbitrary charge in nonsymmetric electrolytes, assuming finite surface conductivity and considering the entire frequency spectrum.

1.2. Interfacial polarization around spherical conductive particles

Garcia et al. (1985) developed a model for conductive spherical particles with insulating shells (for e.g. oxidized surface of pyrite) in a conductive medium where the diffusive effects play an important role. Grosse and Barchini (1992) improved the previous theory for infinitely conductive spherical particles in bulk electrolyte by considering ion flow across the interface. Moreover, in comparison to dielectric mixture formulas, Tuncer et al. (2001) applied a finite element method on cylinder-like conductive inclusion phase to investigate the dielectric relaxation phenomena. Their result shows the two methods match well at low inclusion concentrations. However, as the concentration of inclusion increases, mutual interaction of the inclusions becomes significant.

2. Methodology

2.1. Assumptions

Both the SCAIP model and PPIP model are based on the Poisson-Nernst-Planck (PNP) equations for a dilute solution in a weak electrical

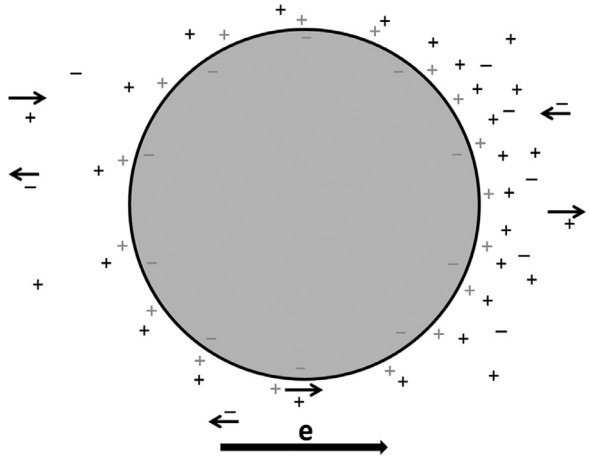

Fig. 1. Cross-section of a nonconductive spherical inclusion possessing surface charge surrounded by an ionic host medium. The inclusion is negatively charged, surrounded by a positive charged counterion layer, which forms a Gouy–Chapman model. Charge carriers in the ionic host medium are cations, identified by "+" symbol, and anions, identified by "−" symbol. The direction of the externally applied electrical field, **e**, is identified with a bold arrow next to the symbol "**e**". The direction of movement of the charge carriers in the ionic host medium is represented by the arrow next to the symbol of the charge carrier.

field regime. By applying the PNP equations, we analyze the EM response of a representative volume comprising a single, isolated nonconductive inclusion possessing surface charge or electrically conductive inclusion surrounded by an electrolyte-saturated host medium (Zheng and Wei, 2011). To simplify the model, we assume only spherical particles are present in the porous media. Also, the host, inclusion, and pore-filling fluid are assumed to have homogeneous, isotropic, and nondispersive electrical properties. Therefore, the frequency dispersion and dielectric enhancement predicted by the SCAIP model or PPIP model solely stems from the SCAIP or PPIP phenomena around the negatively charged nonconductive or electrically conductive inclusions. We also assume all the charge carriers bear unitary charge and both host and inclusion phases bear binary, symmetric charge carriers.

2.2. Mechanistic model of interfacial polarization due to surface-charge-bearing spherical nonconductive particle

The surface of a nonmetallic (nonconductive) mineral, such as clay, acquires charges if the mineral is surrounded by electrolytes due to ionic adsorption, protonation/deprotonation of the hydroxyl groups, and dissociation of other potentially active surface groups, also combinedly referred as surface complexation reactions (Leroy and Revil, 2004). In this paper, surface-conductance-assisted interfacial polarization (SCAIP) model is developed to investigate the interfacial polarization phenomena around surface-charge-bearing spherical nonconductive particles. Fig. 1 shows SCAIP phenomena in a representative volume of a dilute mixture of uniformly distributed surface-charge-bearing nonconductive spherical inclusions in an electrolyte-saturated host medium, where interfacial polarization is independent of the direction of the externally applied electric field due to spherical symmetry.

The phenomenological basis of interfacial polarization considered in our work builds on the mechanistic descriptions outlined by Grosse (1988). The negatively charged inclusion, together with its positive counterion layer, essentially behaves as a conductor of positive charge carriers, which allows the positive ions in the host medium to freely exchange with the ions in the counterion layer, and as a nonconductor of negative charges, which excludes the negative ions from the counterion layer.

In the absence of an externally applied electric field, a Gouy–Chapman double layer is assumed around the surface-charge-bearing nonconductive inclusions, where the positive counterion layer is characterized by a finite surface conductivity. We assume the thickness of counterion layer is negligible, which is valid when $a \gg \lambda_D$, where λ_D is the Debye screening length and a is the characteristic length of the inclusion phase.

2.2.1. Development of SCAIP model

The Poisson–Nernst–Planck (PNP) equation has been used to model electromigration and diffusion of ionic charge carriers in electrolytes (Zheng and Wei, 2011) and that due to holes and electrons in semiconductors (Schmuck and Bazant, 2015). It is based on a mean-field approximation of charge carrier interactions and continuum descriptions of charge concentration and electrostatic potential. We apply the PNP equations to model charge dynamics and relaxation in the representative volume containing only two phases: the host medium, denoted by subscript h, and the conductive (to be discussed in the following section) or nonconductive particles (inclusions), denoted by subscript i. In our formulation, the host medium can be assumed as a homogeneous mixture of electrolyte and nonconductive matrix or as a pure electrolyte. At time $t < 0$, it is assumed that there is no external electric field exciting the representative volume. Initial charge carrier densities at equilibrium conditions in both the host and inclusion phases are denoted as $N^{\pm}_{0,j}$, where subscript j takes the form of i for the inclusion phase and h for the host phase. Starting at time $t = 0$, the representative volume experiences a uniform externally applied electric field $E = E_0 e^{i\omega t}$, where E_0 is the amplitude of the externally applied electric field, i is square root of -1, ω is the angular frequency (rad/s) of the externally applied electric field, and e is Euler's number. Note $\omega = 2\pi f$, where f is frequency (Hz). We assume the negatively charged spherical nonconductive particle is surrounded by a layer of positively charged, conducting counterion layer, which has a surface conductance λ and bears a field-induced surface charge density $\rho e^{i\omega t}\cos\theta$, where θ is the angle between the normal to the interface and the incident external electric field. Under a weak field approximation, charge carrier densities in host and inclusion phases are perturbed from their equilibrium conditions near the host-inclusion interfaces, resulting in a new linearly approximated charge distribution, given by

$$N^{\pm}_j(r,t,\theta) = N^{\pm}_{0,j} + c^{\pm}_j(r)e^{i\omega t}\cos\theta \tag{1}$$

such that $|c^{\pm}_j| \le N^{\pm}_{0,j}$, $c^{\pm}_j$ is the charge density variation near the host-inclusion interface in medium j due to the externally applied electric field and r is the radial distance along the normal to the interface. Note that in this section, for nonconductive inclusion, $c^{\pm}_i(r) = 0$. In addition, one assumption is the absence of charge carriers in the nonconductive inclusion phase, $N^{\pm}_{0,i} = 0$. Further, the symbol "+" identifies positive-charge carriers such as holes and cations, while the symbol "−" identifies negative-charge carriers such as electrons and anions.

We assume that the characteristic length a of the inclusions phase is far greater than the Debye screening length λ_D. Note that λ_D is a measure of induced charge distribution that forms around an inclusion particle due to surface charges that exist on the inclusion particle in the absence of an externally applied electric field. In other words, λ_D represents a volume outside of which surface charges on an inclusion particle are electrically screened. The characteristic length a is equal to the radius of spherical inclusion. Mathematically, $\lambda_D = \sqrt{\varepsilon_h k_B T/(2Z^+_h Z^-_h q^2 N_{0,h})}$, where ε_h is dielectric permittivity of the host, k_B is Boltzmann's constant, T is absolute temperature, $Z^{\pm}_h$ is charge number of positive and negative charge carriers in the host, and q is the elementary charge. The volume fraction of conductive (for e.g., pyrite) and nonconductive particles (for e.g. clays) is assumed to be in the range of 5–15%. Another simplifying assumption is that all the charge carriers bear unitary charge and that both host and inclusion phases bear binary, symmetric charge carriers.

In other words,

$$Z_j^{\pm} = 1,\ \mu_h^+ = \mu_h^- = \mu_h,\ \mu_i^+ = \mu_i^- = \mu_i,\ N_{0,i}^+ = N_{0,i}^- = N_{0,i},\quad N_{0,h}^+ = N_{0,h}^- = N_{0,h} \tag{2}$$

where $\mu_j^{\pm}$ is the electrical mobility of positive and negative charge carriers in medium j, and $Z_j^{\pm}$ is charge number of positive and negative charge carriers in medium j.

The current density of each charge carrier type in the host and inclusion phases is the sum of current density due to drift current and diffusion current. In the absence of generation/recombination reactions, the transport equation representing conservation laws for charge-carrying species can be written as

$$\boldsymbol{j}_j^{\pm} = \boldsymbol{j}_{j,drift}^{\pm} + \boldsymbol{j}_{j,diffusion}^{\pm} = qN_j^{\pm}\mu_j \boldsymbol{e}_j \mp qD_j^{\pm}\nabla N_j^{\pm} \tag{3}$$

where $\boldsymbol{j}_j^{\pm}$ is the current density of positive and negative charge carriers, respectively, in medium j, $\mathbf{e}_j$ is the net electric field vector in medium j, and $D_j^{\pm}$ is diffusion coefficient of positive and negative charge carriers, respectively, in medium j. When using the simplifying assumption for electrical mobility of charge carriers, as mentioned in Eq. (2), and Einstein's relationship of diffusion coefficient with electrical mobility, namely $D_j = (\mu_j k_B T)/q$, we obtain

$$D_h^+ = D_h^- = D_h;\ D_i^+ = D_i^- = D_i \tag{4}$$

By substituting $\boldsymbol{e}_j = -\nabla\varphi_j$ into the low-frequency limit of Maxwell's equations (induction neglected) and substituting Eq. (4) into Eq. (3), we express the charge species conservation condition as

$$\boldsymbol{j}_j^{\pm} = -qN_j^{\pm}\mu_j\nabla\varphi_j \mp qD_j\nabla N_j^{\pm} \tag{5}$$

where φ_j is the electrical potential in medium j. Eq. (5) is Nernst–Planck's equation that describes the relationship of the flux of charge-carrying species to its concentration gradient and that to the applied electrical potential gradient in a given medium. Nernst-Planck's equation can alternatively be expressed as

$$\boldsymbol{j}_j^{\pm} = -D_j^{\pm}N_j^{\pm}\nabla\varphi_{cj}^{\pm} \tag{6}$$

where $\varphi_{cj}^{\pm} = k_B T \ln N_j^{\pm} \pm qZ_j^{\pm}\varphi_j$ is the electrochemical potential of charge carriers. The continuity equation for charge carrier density based on mass conservation for each charge carrier type in an incompressible medium without any convective flow can be written as

$$\mp q\frac{\partial N_j^{\pm}}{\partial t} = \nabla\cdot\boldsymbol{j}_j^{\pm} \tag{7}$$

By applying Eqs. (5)–(7), we obtain

$$\frac{\partial N_j^+}{\partial t} = \nabla\cdot\left(D_j\nabla N_j^+ + \mu_j N_j^+\nabla\varphi_j\right) \tag{8}$$

and

$$\frac{\partial N_j^-}{\partial t} = \nabla\cdot\left(D_j\nabla N_j^- - \mu_j N_j^-\nabla\varphi_j\right) \tag{9}$$

The time derivative of Eq. (1) assuming axial symmetry is

$$\frac{\partial N_j^{\pm}}{\partial t} = i\omega c_j^{\pm} \tag{10}$$

where $c_j^{\pm} = c_j^{\pm}(r,t,\theta) = c_j^{\pm}(r)e^{i\omega t}\cos\theta$. We apply Eq. (10) to Eqs. (8) and 9, then we add and subtract Eqs. (8) and (9) to obtain Eqs. (11) and (12) expressed as:

$$-iq\omega d_j = -2qN_{0,j}\mu_j\Delta\varphi_j - qD_j\Delta d_j \tag{11}$$

and

$$-iq\omega s_j = -qD_j\Delta s_j \tag{12}$$

where $d_j = c_j^+ - c_j^-$ represents net charge density variation, $s_j = c_j^+ + c_j^-$ represents total ion density variation, and Δ (∇^2) is Laplace's operator. Note d_j and s_j are finite everywhere in the representative volume, and for nonconductive particles, $d_i = s_i = 0$. We obtained Eqs. (11) and (12) by assuming $d_j\mu_j \ll 1$ and $s_j\mu_j \ll 1$ as $|c_j^{\pm}| \le N_{0,j}^{\pm}$.

Under the influence of an externally applied EM field, the distribution of charge carriers in both media leads to a time-varying electric potential that is expressed as $\varphi_j(r,t,\theta) = \varphi_j(r)e^{i\omega t}\cos\theta$. Using Gauss's law and Eq. (1), we obtain

$$\nabla\cdot\left(\varepsilon_j\boldsymbol{e}_j\right) = P_{f,j} = q\left(N_j^+ - N_j^-\right) = q\left(c_j^+ - c_j^-\right) = qd_j \tag{13}$$

where $P_{f,j}$ is the net free charge density in medium j due to charge redistribution in the presence of an externally applied EM field, $\boldsymbol{e}_j$, and $\varepsilon_j = \varepsilon_{r,j}\varepsilon_0$ is the dielectric permittivity of medium j, $\varepsilon_{r,j}$ is the relative permittivity of medium j, and $\varepsilon_0 = 8.854\times10^{-12}$F/m is the vacuum permittivity. Eq. (13) relates the spatial distribution of electric charge to the time-varying electric field. Assuming both media are linear, isotropic, and homogeneous, and that the electric field can be defined by a scalar electrical potential field, φ_j, we obtain

$$\nabla\cdot\left(\varepsilon_j\boldsymbol{e}_j\right) = -\nabla\cdot\left(\varepsilon_j\nabla\varphi_j\right) = -\varepsilon_j\Delta\varphi_j \tag{14}$$

By combining Eqs. (13) and (14), we obtain an alternate expression of Poisson's equation, expressed as

$$\Delta\varphi_j = -\frac{qd_j}{\varepsilon_j} \tag{15}$$

Poisson's equation is applied to describe the electric field in terms of the electrical potential, the gradient of which governs electromigration in both media. By substituting Eq. (15) into Eq. (11), we obtain the Poisson-Nernst-Planck (PNP) equation, given by

$$-iq\omega d_j = 2q^2N_{0,j}\mu_j d_j/\varepsilon_j - qD_j\Delta d_j \tag{16}$$

which can be re-written as

$$\Delta d_j = \left(\frac{i\omega}{D_j} + \frac{\sigma_j}{\varepsilon_j D_j}\right)d_j \tag{17}$$

where $\sigma_j = 2N_{0,j}\mu_j q$ is the electrical conductivity of medium j. We rewrite Eqs. (17) and (12) as

$$\Delta d_j = {\gamma_j}^2 d_j \tag{18}$$

where

$${\gamma_j}^2 = \left(\frac{i\omega}{D_j} + \frac{\sigma_j}{\varepsilon_j D_j}\right) \tag{19}$$

and

$$\Delta s_j = {\xi_j}^2 s_j \tag{20}$$

where

$${\xi_j}^2 = \frac{i\omega}{D_j} \tag{21}$$

respectively. Eqs. (18) and (20) are Helmholtz partial differential equations (PDE) which can be solved to obtain distinct analytical expressions of d_j and s_j for the host and inclusion phases, respectively. Eq. (18) is inserted into Eq. (15) to obtain the following Laplace PDE that can be solved for the electric potential field in the representative volume:

$$\Delta\vartheta_j = 0 \tag{22}$$

where

$$\vartheta_j = \varphi_j + \left(qd_j\right)/\left(\gamma_j^2\varepsilon_j\right) \tag{23}$$

2.2.2. Solution of Helmholtz PDE

As mentioned before, for nonconductive inclusions, $d_i = s_i = 0$. So, we're solving the Helmholtz PDEs to obtain the distinct analytical expressions of d_h and s_h for the host phase. A sphere of radius equal to a exhibits dipolarizability (dipole moment) in the radial direction. Such an inclusion identifies a grain or vug. In order to compute the dipolarizability of the representative volume comprising a spherical inclusion

in an electrolytic host, Eq. (18) can be expressed in spherical coordinates, assuming azimuthal symmetry, axial symmetry, and a separable solution (Young, 2009) for $d_h(r,\theta) = R_h(r)T_h(\theta)$, as

$$\frac{1}{R_h}\frac{\partial}{\partial r}\left(r^2\frac{\partial R_h}{\partial r}\right) - \gamma_h^2 r^2 + \frac{1}{T_h \sin\theta}\frac{\partial}{\partial\theta}\left(\frac{\sin\theta\partial T_h}{\partial\theta}\right) = 0 \tag{24}$$

and

$$\frac{1}{\sin\theta}\frac{\partial}{\partial\theta}\left(\frac{\sin\theta\partial T_h}{\partial\theta}\right) = -n(n+1)T_h \tag{25}$$

where n is an integer referring to the order of the standing wave solution. A standing wave solution (Young, 2009) to the above differential equation is

$$T_h = \sum_{n=1}^{\infty}\left[A_{n,h}P_n^0(\cos\theta) + B_{n,h}Q_n^0(\cos\theta)\right] \tag{26}$$

where P_n^0 and Q_n^0 are associated Legendre functions of the first and second kind (Weisstein, 2018a), respectively, of nth order and $A_{n,h}$ and $B_{n,h}$ are unknown complex-valued coefficients of the general solution of the partial differential Eq. (25). Substituting Eq. (25) in Eq. (24), we obtain

$$\frac{\partial}{\partial r}\left(r^2\frac{\partial R_h}{\partial r}\right) - \left[\gamma_h^2 r^2 + n(n+1)\right]R_h = 0 \tag{27}$$

A standing wave solution to the above differential equation is

$$R_h = \sum_{n=1}^{\infty}\left[C_{n,h}i_n(r\gamma_h) + D_{n,h}k_n(r\gamma_h)\right] \tag{28}$$

where n is an integer for the standing wave solution (Young, 2009), i_n and k_n are the modified spherical Bessel function of the first and second kind (Weisstein, 2018b), respectively, of $n-$th order. $C_{n,h}$ and $D_{n,h}$ are unknown complex-valued coefficients of the general solution of the partial differential Eq. (27). i_n and k_n can be expressed in terms of modified Bessel function of the first and second kind, respectively, as $i_n(r\gamma_h) = \sqrt{\frac{\pi}{2r\gamma_h}}I_{n+\frac{1}{2}}(r\gamma_h)$ and $k_n(r\gamma_h) = \sqrt{\frac{2}{\pi r\gamma_h}}K_{n+\frac{1}{2}}(r\gamma_h)$, where $I_{n+\frac{1}{2}}$ and $K_{n+\frac{1}{2}}$ are the modified Bessel function of the first and second kind, respectively, of $(n+\frac{1}{2})-$th order. In the analytical expression of our model, the series is reduced to a single term for $n=1$ and $B_{n,h}=0$ by considering the following symmetries of the charge density: (1) axial symmetry, (2) anti-symmetry with respect to θ, (3) uniformity of the external applied field, and (4) dipolar nature of the externally applied field. This simplification is aligned with boundary conditions that cannot be satisfied by other values of n. This reduces Eqs. (28) and (26) to

$$R_h = C_h i_1(r\gamma_h) + D_h k_1(r\gamma_h) \tag{29}$$

and

$$T_h = A_h\cos\theta \tag{30}$$

respectively, where C_h, D_h, and A_h and are unknown complex-valued coefficients of the particular solution obtained from Eqs. (26) and (28). The general representation of $d_h(r,\theta)$ can now be written, by combining Eqs. (29) and (30), as

$$d_h(r,\theta) = A_h\left[C_h i_1(r\gamma_h) + D_h k_1(r\gamma_h)\right]\cos\theta \tag{31}$$

Using the condition that $d_h(r,\theta)$ should be finite at $r\to\infty$, we obtain a particular solution of d_h for the host phase that can be represented as

$$d_h(r,\theta) = B_{h1}k_1(r\gamma_h)\cos\theta \tag{32a}$$

or

$$d_h(r,\theta) = B_{h1}\left[e^{-r\gamma_h}\left(\frac{1}{r\gamma_h} + \frac{1}{(r\gamma_h)^2}\right)\right]\cos\theta \tag{32b}$$

where B_{h1} is unknown complex-valued coefficient of the particular solution in the host medium obtained from Eq. (31). Note when $r\to\infty$, $d_h(r,\theta)=0$. Repeat the above procedure, we can obtain a particular solution of s_h for the host phase from Eq. (20) that can be represented as

$$s_h(r,\theta) = B_{h2}k_1(r\xi_h)\cos\theta \tag{33a}$$

or

$$s_h(r,\theta) = B_{h2}\left[e^{-r\xi_h}\left(\frac{1}{r\xi_h} + \frac{1}{(r\xi_h)^2}\right)\right]\cos\theta \tag{33b}$$

where B_{h2} is unknown complex-valued coefficient of the particular solution in the host medium.

2.2.3. Solution of Laplace PDE

The Laplacian partial differential equation (PDE) must be solved to obtain the electric potential field in the representative volume. Assuming azimuthal symmetry and a separable solution for $\vartheta_j(r,\theta,\varphi) = R_{\varepsilon j}(r)T_{\varepsilon j}(\theta)$, Eq. (22) can be expressed in spherical coordinates as

$$\Delta\vartheta_j = \frac{1}{R_{\varepsilon j}}\frac{\partial}{\partial r}\left(r^2\frac{\partial R_{\varepsilon j}}{\partial r}\right) + \frac{1}{T_{\varepsilon j}\sin\theta}\frac{\partial}{\partial\theta}\left(\frac{\sin\theta\partial T_{\varepsilon j}}{\partial\theta}\right) = 0 \tag{34}$$

Assuming axial symmetry, a general solution (Hogg, 2001) to the above PDE can be expressed as

$$\vartheta_j(r,\theta) = \sum_{n=0}^{\infty}\left[A_{n,j}r^n + C_{n,j}r^{-(n+1)}\right]\left[E_{n,j}P_n^0(\cos(n\theta)) + F_{n,j}Q_n^0(\sin(n\theta))\right] \tag{35}$$

where n is an integer and $A_{n,j}$, $C_{n,j}$, $E_{n,j}$, and $F_{n,j}$ are unknown complex-valued coefficients of the general solution of the PDE expressed in Eq. (34). For the analytical modeling purposes, we assume $n=1$, $F_{n,j}=0$, $A_{0,j}=0$ and $C_{0,j}=0$, which ensures that the remaining terms satisfy the polar angle dependence of the model. Simplified representation of Eq. (35) is expressed as

$$\vartheta_j(r,\theta) = \left(A_{1,j}r + C_{1,j}r^{-2}\right)E_{1,j}\cos\theta \tag{36a}$$

which can be rewritten using Eq. (23) as

$$\varphi_j(r,\theta) = \left(A_j r + C_j r^{-2}\right)\cos\theta - \frac{q d_j(r,\theta)}{\gamma_j^2\varepsilon_j} \tag{36b}$$

Using the condition that $d_i=0$ and φ_i should be finite when $r\to 0$, we can obtain $C_i=0$. So, a standing wave representation of Eq. (36b) for the nonconductive inclusion phase is

$$\varphi_i(r,\theta) = A_i r\cos\theta \tag{37}$$

where A_i is unknown complex-valued coefficient of the particular solution in the nonconductive inclusion phase obtained from Eq. (36b). Using the condition when $r\to\infty$, $d_h=0$, we can obtain $A_h=-E_0$. A standing wave representation of Eq. (36b) for the host phase, using Eq. (32b), is

$$\varphi_h(r,\theta) = \left(-E_0 r + C_h r^{-2}\right)\cos\theta - \frac{qB_{h1}}{\gamma_h^2\varepsilon_h}\left[e^{-r\gamma_h}\left(\frac{1}{r\gamma_h} + \frac{1}{(r\gamma_h)^2}\right)\right]\cos\theta \tag{38}$$

where C_h is unknown complex-valued coefficient of the particular solution in the host obtained from Eq. (36b) and E_0 is the amplitude of the externally applied electric field.

2.2.4. Boundary conditions

To obtain an expression for the dipolarizability (dipole moment), we need first to identify the boundary conditions (Grosse, 1988):

(a) Continuity of the electric potential at the interface.

$$\varphi_i(r=a) = \varphi_h(r=a) \tag{39a}$$

(b) Discontinuity of the normal component of the displacement current at the interface because of the surface charge distribution on the inclusion phase. This boundary condition is derived from Gauss' Law.

$$\varepsilon_i \left.\frac{\partial \varphi_i}{\partial r}\right|_{r=a} - \varepsilon_h \left.\frac{\partial \varphi_h}{\partial r}\right|_{r=a} = \rho \cos\theta \tag{39b}$$

(c) Continuity of the surface charge density at the host-inclusion interface qualitatively expressed as: Rate of change of surface charge density normal drift/conduction current at the interface due to potential gradient arising from the external electromagnetic field + normal diffusion current due to concentration gradient in the host media at the interface + tangential conduction current due to the potential gradient arising from the surface-charge-bearing inclusion phase. In other words, this boundary condition shows that the time derivative of surface charge density in the counterion layer is equal to the sum of the normal conduction and diffusion current due to potential and concentration difference, separately, from the host medium and the tangential conduction current due to potential from the inclusion phase.

$$-i\omega\rho\cos\theta = -\frac{\sigma_h}{2}\left.\frac{\partial \varphi_h}{\partial r}\right|_{r=a} - qD_h \left.\frac{\partial c_h^+}{\partial r}\right|_{r=a} + \frac{2\lambda}{a} A_i \cos\theta \tag{39c}$$

(d) The normal component of the current density of negative ions in the host medium must vanish at the interface due to the assumption that the negative ions are excluded from the counterion layer.

$$J_h^- = -\frac{\sigma_h}{2}\left.\frac{\partial \varphi_h}{\partial r}\right|_{r=a} + qD_h \left.\frac{\partial c_h^-}{\partial r}\right|_{r=a} = 0 \tag{39d}$$

(e) Due to the application of the external electric field, we use a simplifying assumption that the relative change of the positive ion density in the counterion layer (which is assumed to be negligibly thin) and that in the host medium must be the equal because the positive ions in the host medium can freely exchange with the ions in the counterion layer.

$$\frac{c_h^+(r=a,\theta)}{N_{0,h}} = \frac{\rho\cos\theta}{\rho_0} \tag{39e}$$

where ρ_0 is the initial equilibrium surface change density in the counterion layer and ρ is the net resultant surface charge density in the counterion layer after the application of electric field.

2.2.5. Solution for the Dipolarizability

Using boundary condition (39a), Eqs. (37) and (38) can be equated on the surface of the sphere of radius equal to a. The resulting equation can be abbreviated as

$$-E_0 a + \frac{C_h}{a^2} - E_h B_{h1} = A_i a \tag{40a}$$

where

$$E_h = \frac{q}{\gamma_h^2 \varepsilon_h} e^{-a\gamma_h}\left[\frac{1}{a\gamma_h} + \frac{1}{(a\gamma_h)^2}\right] \tag{40b}$$

The equation obtained using boundary condition (39b) at the surface of the sphere can be abbreviated as

$$\varepsilon_h\left(E_0 + \frac{2C_h}{a^3} - G_h B_{h1}\right) + \varepsilon_i A_i = \rho \tag{41a}$$

where

$$G_h = \frac{q}{\gamma_h \varepsilon_h} e^{-a\gamma_h}\left[\frac{1}{a\gamma_h} + \frac{2}{(a\gamma_h)^2} + \frac{2}{(a\gamma_h)^3}\right] \tag{41b}$$

Boundary condition (39c) gives us the following abbreviated equation:

$$i\omega\rho = -\frac{\sigma_h}{2}E_0 - \frac{\sigma_h C_h}{a^3} + \frac{\sigma_h}{2}G_h B_{h1} - \frac{D_h}{2}\gamma_h^2 G_h B_{h1}\varepsilon_h - \frac{D_h}{2}\xi_h^2 L_h B_{h2}\varepsilon_h - \frac{2\lambda}{a}A_i \tag{42a}$$

where

$$L_h = \frac{q}{\xi_h \varepsilon_h} e^{-a\xi_h}\left[\frac{1}{a\xi_h} + \frac{2}{(a\xi_h)^2} + \frac{2}{(a\xi_h)^3}\right] \tag{42b}$$

Similarly, the equation obtained using boundary condition (39d) can be abbreviated as

$$\frac{\sigma_h}{2}E_0 + \frac{\sigma_h C_h}{a^3} - \frac{\sigma_h}{2}G_h B_{h1} = \frac{D_h}{2}\xi_h^2 L_h B_{h2}\varepsilon_h - \frac{D_h}{2}\gamma_h^2 G_h B_{h1}\varepsilon_h \tag{43}$$

For boundary condition (39e), we assume the electrical mobilities in the two regions are the same to re-write this boundary condition as

$$2qc_h^+(r=a) = \frac{\rho\sigma_h}{\lambda} \tag{44}$$

After solving Eqs. (40a), (41a), (42a), (43) and (44), we obtain the dipolarizability (dipolar field coefficient) of the representative volume comprising a spherical nonconductive inclusion in an electrolytic host as

$$f_{ncond}(\omega) = \frac{C_h}{E_0 a^3} = \frac{Q(R+A)-P}{Q(R-2A)+2P} \tag{45}$$

where

$$A = \frac{1}{a^2} \tag{45a}$$

$$P = \gamma_h^2 + \xi_h^2\frac{G}{H} + \frac{2G}{a^2 L} \tag{45b}$$

$$Q = \frac{1}{iF+1}\left[2 - \frac{a^2\xi_h^2}{H}\left(\frac{L}{iF}+E\right) - \frac{2E}{L}\right] \tag{45c}$$

$$R = \frac{P}{Q}\left(\frac{iFE+L}{iF+1}\right) \tag{45d}$$

$$H = \frac{aL_h}{F_h},\ G = \frac{aG_h}{E_h},\ L = \frac{2\lambda}{a\sigma_h},\ E = \frac{\varepsilon_i}{\varepsilon_h},\ F = \frac{\omega\varepsilon_h}{\sigma_h} \tag{45e}$$

$$F_h = \frac{q}{\xi_h^2 \varepsilon_h} e^{-a\xi_h}\left[\frac{1}{a\xi_h} + \frac{1}{(a\xi_h)^2}\right] \tag{45f}$$

2.3. Mechanistic model of interfacial polarization due to spherical conductive particle

In this paper, perfectly polarized interfacial polarization (PPIP) model is applied to investigate interfacial polarization phenomena around conductive particle. Fig. 2 shows PPIP phenomena in a representative volume of a dilute mixture of uniformly distributed electrically conductive spherical inclusions in an electrolyte-saturated host medium, where interfacial polarization is independent of the direction of the externally applied electric field due to spherical symmetry.

The phenomenological basis of interfacial polarization considered in our work builds on the mechanistic descriptions outlined by Revil et al. (2015). Charge carriers in conductive minerals have higher mobility compared to ions in porous geomaterials. In the presence of an externally applied EM field, charge carriers in the disseminated electrically conductive inclusions migrate faster and accumulate at impermeable interfaces. Consequently, electrically conductive inclusions behave as dipoles in the presence of an externally applied electric field. Subsequently, charge carriers in the host medium migrate and accumulate on host-inclusion interfaces under the influence of the externally applied electric field and that of the induced charges in conductive inclusions.

In the absence of an externally applied electric field, a negligible initial surface charge is assumed on electrically conductive inclusions. Thus, there is typically a negligible double layer around the surface of electrically conductive inclusions, whereby the surface conductance of a conductive inclusion is negligible. Similar assumptions are made in electrochemistry and colloid science with respect to electrochemical relaxation around metallic surfaces (Chu and Bazant, 2006). Also, we assume absence of redox-active species and neglect the influence of pH of

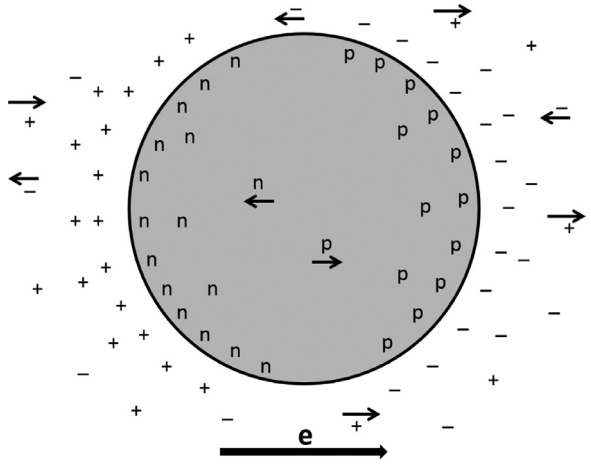

Fig. 2. Cross-section of a perfectly polarized conductive spherical inclusion surrounded by an ionic host medium. Charge carriers in the ionic host medium are cations, identified by "+" symbol, and anions, identified by "–" symbol. Charge carriers in the conductive spherical inclusion are n- and p-charge carriers, identified by symbol "n" and "p", respectively. The direction of the externally applied electrical field, **e**, is identified with a bold arrow next to the symbol "**e**". The direction of movement of the four different types of charge carriers is represented by the arrow next to the symbols of the charge carriers.

pore water (Revil et al., 2015). The host and inclusion phases can be modeled as an electrically conductive, insulating, or dielectric material. Also, pore-filling fluid can be modeled as electrically conductive (e.g. brine) or non-conductive material (e.g. oil).

2.3.1. Development of PPIP model

The development of the PPIP model (Misra et al., 2016b) is very similar to that of the SCAIP model. For PPIP model development, spontaneous initial accumulation of charges is assumed to be absent on the host-inclusion interfaces. At time $t < 0$, electro-neutrality is assumed throughout the system.

2.3.2. Solution of Helmholtz PDE

The above-mentioned Eq. (18) must be solved to obtain an analytical expression for d_j in the host and inclusion phases around the perfectly polarized host-inclusion interface of conductive spherical inclusion. Recall that $d_j = c_j^+ - c_j^-$ represents net charge density variation, where $c_j^{\pm}$ is the charge density variation near the host-inclusion interface in medium j due to the externally applied electric field. Expression for $d_h(r,\theta)$ for the mixture containing conductive spherical inclusion is the same as that for the mixture containing nonconductive spherical inclusion. Using the condition that $d_i(r,\theta)$ should be finite at $r \to 0$, we obtain a particular solution for d_i for the mixture containing conductive spherical inclusion that can be represented as

$$d_i(r,\theta) = B_i i_1(r\gamma_i)\cos\theta \tag{46a}$$

or

$$d_i(r,\theta) = B_i\left[\frac{\cos h(r\gamma_i)}{r\gamma_i} - \frac{\sin h(r\gamma_i)}{(r\gamma_i)^2}\right]\cos\theta \tag{46b}$$

where B_i is unknown complex-valued coefficient of the particular solution in the inclusion phase obtained from Eq. (31), substituting the subscript h with i. Note when $r \to 0$, it is assumed that $d_i(r,\theta) = 0$.

2.3.3. Solution of Laplace PDE

The above-mentioned Eq. (22) must be solved to obtain the electric potential field in the representative volume. The expression for $\varphi_h(r,\theta)$ for the mixture containing conductive spherical inclusion is the same as that for the mixture containing nonconductive spherical inclusion. Using the condition when $r \to 0$, $d_i = 0$ and φ_i should be finite, we can obtain $C_i = 0$. A standing wave representation of Eq. (36b) for the conductive inclusion phase, using Eq. (46b), is

$$\varphi_i(r,\theta) = A_i r\cos\theta - \frac{qB_i}{\gamma_i^2\varepsilon_i}\left[\frac{\cos h(r\gamma_i)}{r\gamma_i} - \frac{\sin h(r\gamma_i)}{(r\gamma_i)^2}\right]\cos\theta \tag{47}$$

where A_i is unknown complex-valued coefficient of the particular solution in the conductive inclusion phase obtained from Eq. (36b).

2.3.4. Boundary conditions

To obtain an expression for the dipolarizability, we need first to identify the boundary conditions (Grosse and Foster, 1987):

(a) Assuming a zero-intrinsic capacitance of the host-inclusion interface, the electric potential must be continuous at the interface.

$$\varphi_i(r=a) = \varphi_h(r=a) \tag{48a}$$

(b) The normal component of the displacement current must be continuous at the interface. This condition corresponds to the fact that there is no net surface-charge distribution on an electrically conductive inclusion phase.

$$\varepsilon_i \left.\frac{\partial\varphi_i}{\partial r}\right|_{r=a} = \varepsilon_h \left.\frac{\partial\varphi_h}{\partial r}\right|_{r=a} \tag{48b}$$

(c) The normal component of the current density must vanish at the interface for both media. This condition expresses the fact that in the absence of transport of charge carriers and exchange of charges along the interface, the diffusive and electro-migrative currents must cancel each other at the interface. Our focus is perfectly polarizable or completely blocking interfaces without Faradic processes, wherein fluxes of charge carriers must vanish on both sides of the interface. Note that this boundary condition is used to obtain two equations: one for the outer volume of the sphere in the host medium, and the other for the inner volume of the sphere in the inclusion medium.

$$j_j^+ + j_j^- = -2N_{0,j}q\mu_j \left.\frac{\partial\varphi_j}{\partial r}\right|_{r=a} - qD_j \left.\frac{\partial d_j}{\partial r}\right|_{r=a} = 0 \ (j = h \text{ or } i) \tag{48c}$$

2.3.5. Solution for the dipolarizability

Using boundary condition (48a), Eqs. (47) and (38) can be equated on the surface of the sphere of radius equal to a. The resulting equation can be abbreviated as

$$-E_0 a + \frac{C_h}{a^2} - E_h B_h = A_i a - F_i B_i \tag{49a}$$

where

$$F_i = \frac{q}{\gamma_i^2\varepsilon_i}\left[\frac{\cos h(a\gamma_i)}{a\gamma_i} - \frac{\sin h(a\gamma_i)}{(a\gamma_i)^2}\right] \tag{49b}$$

The equation obtained using boundary condition (48b) at the surface of the sphere can be abbreviated as

$$\varepsilon_h\left(-E_0 - \frac{2C_h}{a^3} + G_h B_h\right) = \varepsilon_i\left(A_i + H_i B_i\right) \tag{50a}$$

where

$$H_i = \frac{q}{\gamma_i\varepsilon_i}\left[\frac{2\cos h(a\gamma_i)}{(a\gamma_i)^2} - \frac{\sin h(a\gamma_i)}{a\gamma_i} - \frac{2\sin h(a\gamma_i)}{(a\gamma_i)^3}\right] \tag{50b}$$

Similarly, the equation obtained using boundary condition (48c) at the outer surface of the sphere in the host medium can be abbreviated as

$$C_h = -a^3\left(\frac{E_0}{2} + \frac{i\omega\varepsilon_h G_h B_h}{2\sigma_h}\right) \tag{51}$$

On the other hand, the equation obtained using boundary condition (48c) at the inner surface of the sphere in the inclusion medium can be abbreviated as

$$A_i = \frac{i\omega\varepsilon_i H_i B_i}{\sigma_i} \tag{52}$$

Solve Eqs. (49a), (50a), (51), and (52), we obtain the dipolarizability (dipolar field coefficient) of the representative volume comprising a spherical conductive inclusion in an electrolytic host as

$$f_{cond}(\omega) = \frac{C_h}{E_0 a^3} = -\frac{1}{2} + \frac{3}{2}\frac{i\omega}{\left[\frac{2}{a}\frac{\sigma_h}{\varepsilon_h}\frac{E_h}{G_h} - \frac{2}{a}\frac{\sigma_h^*}{\sigma_i^*}\frac{\sigma_i}{\varepsilon_i}\frac{F_i}{H_i} + i\omega\left(\frac{2\sigma_h^*}{\sigma_i^*}+1\right)\right]} \tag{53}$$

where $\sigma_h^* = \sigma_h + i\omega\varepsilon_h$ is the complex conductivity of the host medium and $\sigma_i^* = \sigma_i + i\omega\varepsilon_i$ is the complex conductivity of the inclusion phase.

2.4. Mechanistic model of complex conductivity of porous media containing nonconductive and conductive particles at various water saturation

We aim to develop a mechanistic model to quantify the conductivity and permittivity (complex conductivity) of geological mixtures containing clay particles, conductive minerals, oil and water. This new model is referred herein as the PPIP-SCAIP (PS) model. To that end, PS model accounts for the interfacial polarization (IFP) due to surface conductance of clays and sands and the IFP due to conductive mineral grains at various water saturations. PS model development requires two steps: first, using PPIP model and SCAIP model to quantify the IFP of the representative volume (as described in Sections 2.2 and 2.3), followed by using effective medium theory to accurately combine the IFP of various representative volumes present in the mixture.

2.4.1. Effective medium theory

We apply the effective-medium theory to determine the effective complex electrical conductivity (σ_{eff}^*) of the mixture (Grosse and Barchini, 1992) after we obtain the expressions of dipolarizability for spherical nonconductive and conductive particles surrounded by the electrolyte-saturated host medium. For the development of our model, as stated in the previous sections, PNP equations are first used to obtain dipolarizabilities (dipole moment), which are microscopic electrical properties, for the representative volume containing either spherical nonconductive or conductive particle. In the derivations of dipolarizabilities, we neglect multipoles effect because their magnitude decreases with inverse power of distance (Sihvola, 2007). Monopole effects are also neglected since there is zero net charge due to the assumed electroneutrality. The macroscopic electrical properties are then computed using effective-medium formulations based on the theory that a material composed of a mixture of distinct homogeneous media can be seen as a homogeneous material at a sufficiently large observation scale (Giordano, 2003).

In this paper, we obtain the effective electrical properties using a Maxwell Garnett type effective-medium formulation. To meet the requirements of the formulation, the volume fraction of nonconductive and conductive inclusions in the mixture should be less than 20% (Revil et al., 2015). Subsurface water-bearing reservoir rocks have less than 10% volume fraction of conductive mineral inclusions but the volume fraction of non-conductive particles possessing surface charge (e.g. clay and sand) can exceed 20%. Moreover, we invoke the PNP equations in the bulk electrolyte that introduces a decaying length scale, where the Maxwell Garnett formula may become invalid at even lower concentration of inclusion phase (Hou et al., 2018). It is also important to mention this formulation used in the calculation neglects the EM interaction between the inclusions and other components. Due to the assumed dilution of the uniformly distributed inclusion phase, individual elements of the dispersed phase are assumed to be isolated and not in contact with each other. Like other mixing theories, our model includes the assumption that the magnitude of spatial variations of the electric field is smaller than the magnitude of variations in the intrinsic electrical properties and geometrical structures. Moreover, all calculations are performed using a quasi-static assumption that requires the size of heterogeneities to be much smaller than the wavelength of the applied EM field (Cosenza et al., 2009). Also, when dealing with a lossy medium, the skin depth of the EM wave must be considered to avoid strong attenuation of the field amplitudes in the conductive heterogeneities. Most importantly, due to the implementation of the PNP equations, our effective-medium formulations unlike other theories (Giordano, 2003) explicitly accounts for the characteristic lengths of heterogeneities, resulting in a physically consistent way to account for the perturbation due to nonconductive or conductive inclusions.

2.4.2. Effective medium theory to quantify the complex conductivity of porous media containing spherical nonconductive and conductive particles

We modified Misra et al. (2016b) effective medium formulation to model the complex conductivity response of multiphase mixtures containing spherical nonconductive and conductive particles, which can be expressed as

$$\frac{\sigma_{\hat{n},eff}^* - \sigma_h^*}{\sigma_{\hat{n},eff}^* + 2\sigma_h^*} = \phi_{cond} f_{cond}(\omega) + \phi_{ncond} f_{ncond}(\omega) \tag{54}$$

where $\sigma^* = \sigma + i\omega\varepsilon$ is a representation of the complex conductivity of a material, $\sigma_{\hat{n},eff}^*$ is the effective complex conductivity of the geological mixture directed along the $\hat{n}$ unit vector that can be measured with an externally applied electric field directed along the $\hat{n}$ unit vector and σ_h^* is the complex-valued conductivity of the homogenous isotropic host material that surrounds the particles. ϕ_{cond} and ϕ_{ncond} is the volume fraction of the conductive and nonconductive inclusion phase in the mixture, respectively. $f_{cond}(\omega)$ and $f_{ncond}(\omega)$ is the dipolarizability of conductive and nonconductive inclusion phase, respectively, along the direction of $\hat{n}$ unit vector, along which the externally applied electric field is directed.

2.4.3. PS model to quantify the complex conductivity of porous media containing spherical nonconductive and conductive particles at various water saturations

All the discussion above assumes that the pores in the host media are 100% saturated with the electrolyte. It is desirable to consider the condition where oil is present along with the electrolyte in the pores of the host medium. In this section, we assume that the oil is distributed as spherical droplets in the mixture and can be treated as nonconductive spherical inclusion phase with negligible surface charge. Also, we assume that the inclusion phases are predominantly water wet. The model developed above (shown as Eq. (54)) is further modified for application at various water saturations, which can be expressed as

$$\frac{\sigma_{\hat{n},eff}^* - \sigma_h^*}{\sigma_{\hat{n},eff}^* + 2\sigma_h^*} = \phi_{cond} f_{cond}(\omega) + \phi_{ncond} f_{ncond}(\omega) + \phi_o f_o(\omega) \tag{55a}$$

where ϕ_o is the volume fraction of oil in the mixture and $f_o(\omega)$ is the dipolarizability of oil, which takes the same form of $f_{ncond}(\omega)$ but with negligible surface charge.

In this paper, we used the model expressed as

$$\frac{\sigma_{\hat{n},eff}^* - \sigma_h^*}{\sigma_{\hat{n},eff}^* + 2\sigma_h^*} = \phi_p f_p(\omega) + \phi_s f_s(\omega) + \phi_c f_c(\omega) + \phi_o f_o(\omega) \tag{55b}$$

where subscripts *p, s, c* and *o* represent pyrite, sand, clay and oil, respectively, to investigate the mixture of pyrite, sand, clay, oil and host electrolyte.

2.4.4. Limitations of the PNP equations used to develop the PS model

A limitation of the PNP equations arises from the omission of the finite volume effect of charge carriers, mutual interactions and steric effects, effects due to transport of ions in confined channels of the pore system, and correlation effects (Chu and Bazant, 2006). Another limitation arises because the model is developed only for symmetric, and binary charge carriers in both the host and inclusion phases. This assumption simplifies the analytical complexity of the PNP formulations. Another drawback of the PNP formulations is that the analysis is performed for materials that contain completely dissociated charge carriers at low concentration values. Moreover, in this paper, unlike Chu and Bazant (2006), we only consider the linear response to weak fields where exact solutions are possible and is closer to the field conditions.

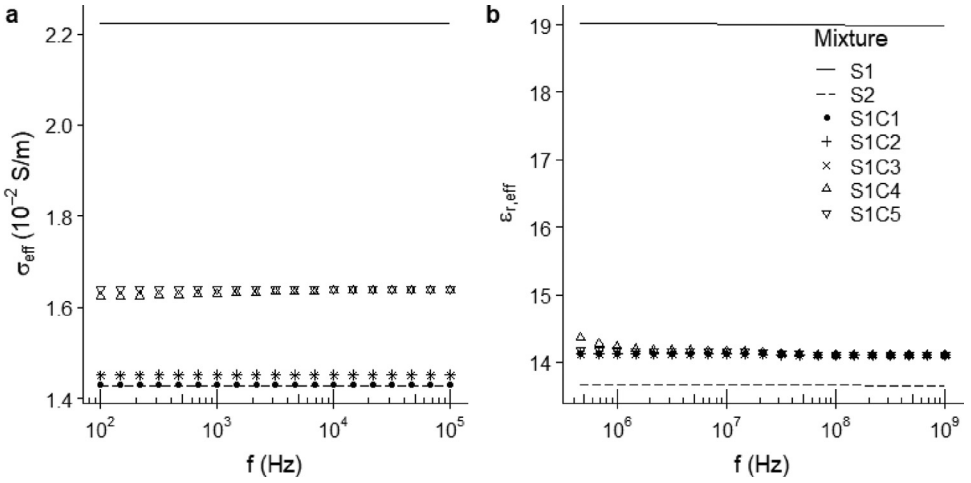

Fig. 3. Comparison of the PS model predictions of (a) σ_{eff} and (b) $\varepsilon_{r,eff}$ of mixtures containing nonconductive spherical sand particles and various types of clay particles (properties listed in Table 1) fully saturated with electrolyte of $\varepsilon_{r,h}$ of 70, σ_h of 0.1 S/m, and D_h of 10^{-9} m^2/s.

Table 1
Properties used for generating Fig. 3, where S1 and S2 represent sand, and C1, C2, and C3 represent three different clay types, and the host is an electrolyte of $\varepsilon_{r,h}$ of 70, σ_h of 0.1 S/m, and D_h of 10^{-9} m^2/s. Typical ε_r of sand and clay ranges from 3 to 5 and 5 to 40, respectively (Martinez and Brynes, 2001). In this paper, we assume ε_r of 4 for sand and 8 for clay.

	ϕ_i (%)	a_i (μm)	$\varepsilon_{r,i}$	λ (S)	a_i/λ
Sand1 (S1)	70	1000	4	10^{-9}	10^{12}
Sand2 (S2)	80	1000	4	10^{-9}	10^{12}
Clay1 (C1)	10	100	8	10^{-8}	10^{10}
Clay2 (C2)	10	10	8	10^{-8}	10^{9}
Clay3 (C3)	10	100	8	10^{-7}	10^{9}
Clay4 (C4)	10	1	8	10^{-8}	10^{8}
Clay5 (C5)	10	100	8	10^{-6}	10^{8}

2.4.5. Limitations of the PPIP and SCAIP models used to develop the PS model

We claim that the PPIP model is reliable for studying the EM response of mixtures containing uniformly distributed conductive particles of characteristic length (a) < 1 mm, conductivity (σ_i) < 10^5 S/m, relative permittivity ($\varepsilon_{r,i}$) < 20, relative magnetic permeability equal to 1, and volume fraction (ϕ_i) < 20% in the frequency range of 100 Hz to 100 MHz. Beyond these limits, the PPIP model predictions will incur significant discrepancies with measurements due to the skin effect of the inclusion phase. The skin effect is primarily governed by the operating frequency and conductivity of the inclusion phase. PPIP model predictions are physically consistent only when the estimated skin depth is an order of magnitude larger than the characteristic length of the particles, where skin depth is defined by the depth from the surface till which an alternating current flow in the conductive particle. For example, at an operating frequency of 100 kHz, an inclusion phase of conductivity of 10^3 S/m and ε_r of 10 exhibits a skin depth of 50 mm. Therefore, the PPIP model can be used to compute the complex conductivity response of a geological mixture containing such an inclusion phase at 100 kHz only when the characteristic length of the inclusion phase is smaller than 5 mm, which is an order of magnitude smaller than the skin depth of 50 mm.

3. Results and discussion

In this section, the effects of PPIP and SCAIP phenomena on low-frequency (100 Hz) σ_{eff} and high-frequency (1 GHz) $\varepsilon_{r,eff}$ prediction are evaluated. The properties of mixtures used for generating plots are summarized in the corresponding tables, where ϕ_i is the volume fraction of a specific phase, a_i is the characteristic length (radius) of spherical particles, D is diffusion coefficient of charge carriers, ε_r is relative permittivity, σ is conductivity, and λ is surface conductance. Property of host medium and inclusion phase are represented with a subscript of h and i, respectively.

3.1. PS model sensitivity to the properties of the nonconductive spherical particles

In this section, we investigate the sensitivity of the PS model predictions of σ_{eff} and $\varepsilon_{r,eff}$ to the properties of surface-charge-bearing nonconductive particles. In Fig. 3, curves S1 and S2 act as the references. Comparing curves S1 against S2, we conclude that the increase in volume fraction of nonconductive particles like sand grains will decrease the σ_{eff} and $\varepsilon_{r,eff}$. Comparing curves S1C4 and S1C5 against S1C1, the decrease of the characteristic length or the increase of the surface conductance of clay particles by two orders of magnitude leads to slight decrease in the σ_{eff} and increase the $\varepsilon_{r,eff}$, as shown in Figs. 3a and 3b, respectively. Moreover, for our model, mixture S1C2 and S1C3 gives the same prediction value for both σ_{eff} and $\varepsilon_{r,eff}$ because the clay particles in both mixtures have the same a_i/λ value and the same relative permittivity. It can also be observed that with the variation in frequency there are negligible dispersion effects on σ_{eff} and $\varepsilon_{r,eff}$.

3.2. PS model sensitivity to the properties of the conductive spherical particles

The mixtures studied in Fig. 4 contain 70% volume fraction of sand and 10% volume fraction of uniformly distributed pyrite. In comparison with the reference curve S1, we can conclude that the presence of conductive particles will increase the $\varepsilon_{r,eff}$ and decrease σ_{eff} at low frequency but will increase σ_{eff} at high frequency. The results show that a higher relative permittivity or conductivity of conductive inclusions, like mixture S1P2 or S1P4, increases σ_{eff} and decreases $\varepsilon_{r,eff}$ of mixture, while a mixture with higher diffusion coefficient like S1P3 decreases σ_{eff} and increases $\varepsilon_{r,eff}$. Moreover, for our model, mixtures S1P1 and S1P5 gives the same prediction for both σ_{eff} and $\varepsilon_{r,eff}$ because both mixtures have the same σ/D value and the same ε_r. Mixture S1P2 and S1P4 also gives the same prediction for both σ_{eff} and $\varepsilon_{r,eff}$ because both mixtures have the same $\sigma\varepsilon_r$ and D. It is also worth to notice that the variation in σ_{eff} prediction only occurs for frequency between 1 kHz and 100 kHz, while the variation in $\varepsilon_{r,eff}$ prediction only occurs for frequency lower than about 5 MHz.

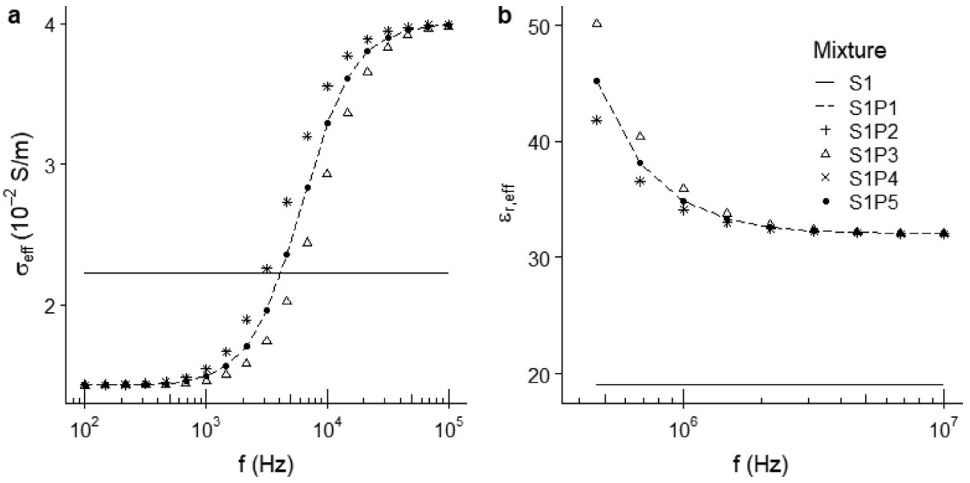

Fig. 4. Comparison of the PS model predictions of (a) σ_{eff} and (b) $\varepsilon_{r,eff}$ of mixtures containing surface-charge-bearing nonconductive spherical sand particles and various types of conductive spherical pyrite particles (properties listed in Table 2) fully saturated with electrolyte of $\varepsilon_{r,h}$ of 70, σ_h of 0.1 S/m and D_h of 10^{-9} m^2/s. Characteristic length of pyrite and sand particles is assumed to be 200 and 1000 μm, and the surface conductance λ of the sand is 10^{-9} S.

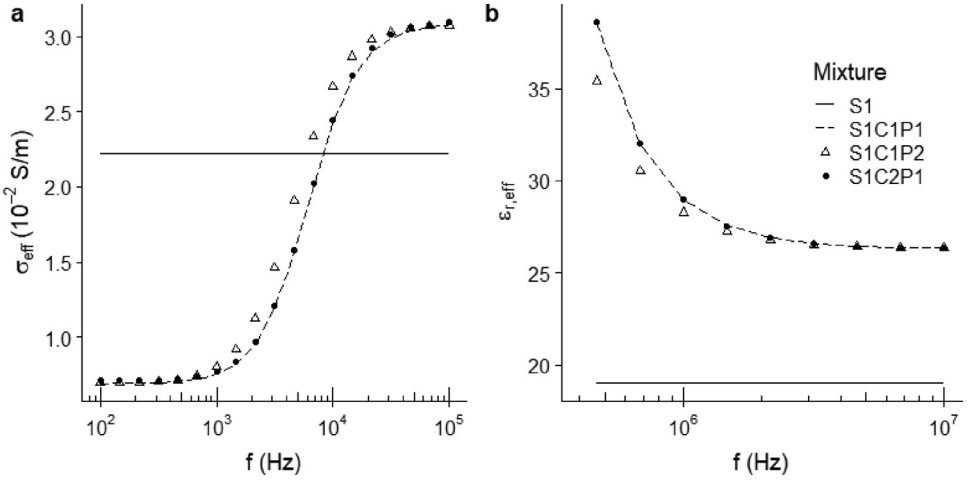

Fig. 5. Comparison of the PS model predictions of (a) σ_{eff} and (b) $\varepsilon_{r,eff}$ of mixtures containing nonconductive spherical sand particles, various types of clay particles, and various types of conductive spherical pyrite particles (properties listed in Table 3) fully saturated with electrolyte of $\varepsilon_{r,h}$ of 70, σ_h of 0.1 S/m and D_h of 10^{-9} m^2/s.

Table 2
Properties used for generating Fig. 4, where S1 represents sand, P1–P5 represent five different pyrite types, and the host is an electrolyte of $\varepsilon_{r,h}$ of 70, σ_h of 0.1 S/m and D_h of 10^{-9} m^2/s.

	ϕ_i (%)	D_i (m^2/s)	$\varepsilon_{r,i}$	σ_i (S/m)	σ_i/D_i	$\sigma_i\varepsilon_{r,i}$
Sand (S1)	70	–	4	–	–	–
Pyrite1 (P1)	10	5×10^{-5}	12	500	10^7	6×10^3
Pyrite2 (P2)	10	5×10^{-5}	24	500	10^7	1.2×10^4
Pyrite3 (P3)	10	10^{-4}	12	500	5×10^6	6×10^3
Pyrite4 (P4)	10	5×10^{-5}	12	1000	2×10^7	1.2×10^4
Pyrite5 (P5)	10	10^{-4}	12	1000	10^7	1.2×10^4

Table 3
Properties used for generating Fig. 5, where S1 represents sand, C1 and C2 represent two different clay types, and P1 and P2 represent two different pyrite types. The host is an electrolyte of $\varepsilon_{r,h}$ of 70, σ_h of 0.1 S/m, and D_h of 10^{-9} m^2/s.

	ϕ_i (%)	a_i (μm)	D_i (m^2/s)	$\varepsilon_{r,i}$	σ_i (S/m)	λ (S)
Sand (S1)	70	1000	–	4	–	10^{-9}
Clay1 (C1)	10	100	–	8	–	10^{-8}
Clay2 (C2)	10	100	–	8	–	10^{-7}
Pyrite1 (P1)	10	200	5×10^{-5}	12	500	–
Pyrite2 (P2)	10	200	5×10^{-5}	12	1000	–

3.3. PS model sensitivity to the mixture of conductive and nonconductive spherical particles

In this section, the PS model predictions of complex conductivity for mixtures containing both nonconductive and conductive inclusions/particles are evaluated. The resulting plots are shown as Fig. 5. Curve S1 act as reference curve representing a clean mixture of sand and electrolyte without any clay and pyrite particles. The presence of uniformly distributed surface-charge-bearing nonconductive and conductive inclusion phases will decrease the σ_{eff} to a value lower than that of clean formation at low frequency (Fig. 5a). This is because at low frequency, the charge carriers quickly reach the equilibrium distribution around the interfaces under the influence of a time-varying electric field, so that the polarized conductive and nonconductive particles act as insulators due to the interface that does not allow charge migration, and hence the reduction in the net electromagnetic energy transport. For frequencies over 1 kHz, the σ_{eff} increases as frequency increases, which will become higher than that of the clean mixture if the frequency is high enough. σ_{eff} saturates for frequencies over 100 kHz. The presence of both nonconductive and conductive inclusion phases will increase the $\varepsilon_{r,eff}$ (Fig. 5b) because the PPIP and SCAIP phenomena leads to larger charge accumulation around the interfaces, and hence higher net electromagnetic energy storage. The $\varepsilon_{r,eff}$ decreases as frequency increases and become stable for frequencies over around 5 MHz. When both conductive and nonconductive spherical inclusions exist in the mixture, the effect of nonconductive inclusions are negligible compared to that of conductive inclusions, which is illustrated by the over-

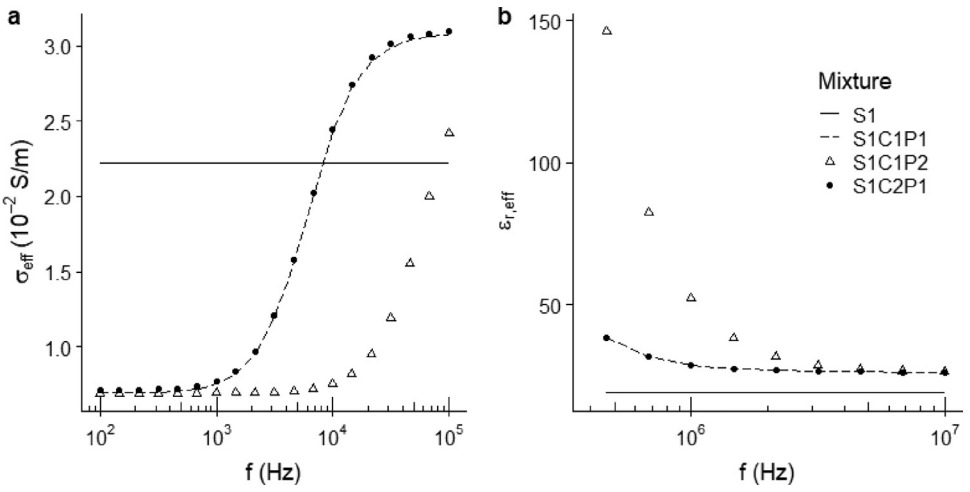

Fig. 6. Comparison of the PS model predictions of (a) σ_{eff} and (b) $\epsilon_{r,eff}$ of mixtures containing spherical sand, clay and pyrite particles of various sizes (properties listed in Table 4) and fully saturated with electrolyte of $\epsilon_{r,h}$ of 70, σ_h of 0.1 S/m and D_h of 10^{-9} m^2/s.

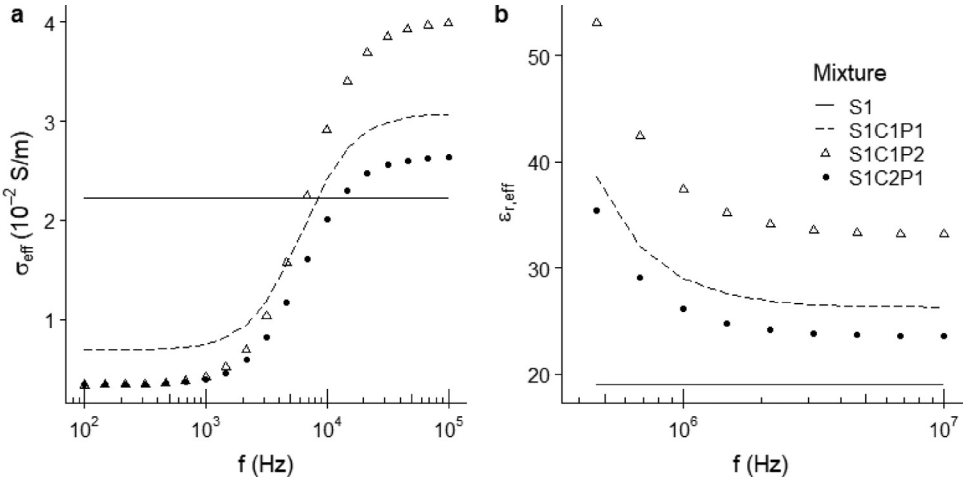

Fig. 7. Comparison of the PS model predictions of (a) σ_{eff} and (b) $\epsilon_{r,eff}$ of mixtures containing spherical sand, clay and pyrite particles at various volume fractions of the inclusion phase (Table 5) and fully saturated with electrolyte of $\epsilon_{r,h}$ of 70, σ_h of 0.1 S/m and D_h of 10^{-9} m^2/s.

Table 4
Properties used for generating Fig. 6, where S1 represents sand, C1 and C2 represent two different clay types, and P1 and P2 represent two different pyrite types and the host is an electrolyte of $\epsilon_{r,h}$ of 70, σ_h of 0.1 S/m and D_h of 10^{-9} m^2/s.

	ϕ_i (%)	a_i (μm)	D_i (m^2/s)	$\epsilon_{r,i}$	σ_i (S/m)	λ (S)
Sand (S1)	70	1000	–	4	–	10^{-9}
Clay1 (C1)	10	100	–	8	–	10^{-8}
Clay2 (C2)	10	10	–	8	–	10^{-8}
Pyrite1 (P1)	10	200	5×10^{-5}	12	500	–
Pyrite2 (P2)	10	20	5×10^{-5}	12	500	–

Table 5
Properties used for generating Fig. 7, where S1 represents sand, C1 and C2 represent clay with different volume fractions, and P1 and P2 represent pyrite with different volume fractions and the host is an electrolyte of $\epsilon_{r,h}$ of 70, σ_h of 0.1 S/m and D_h of 10^{-9} m^2/s.

	ϕ_i (%)	a_i (μm)	D_i (m^2/s)	$\epsilon_{r,i}$	σ_i (S/m)	λ (S)
Sand (S1)	70	1000	–	4	–	10^{-9}
Clay1 (C1)	10	100	–	8	–	10^{-8}
Clay2 (C2)	15	100	–	8	–	10^{-8}
Pyrite1 (P1)	10	200	5×10^{-5}	12	500	–
Pyrite2 (P2)	15	200	5×10^{-5}	12	500	–

lap of S1C1P1 and S1C2P1. In other words, the physical properties of conductive inclusions dominate the predictions.

3.4. PS model sensitivity to the characteristic lengths of conductive and nonconductive spherical particles

In this section, the PS model predictions of complex conductivity for mixtures containing both nonconductive and conductive inclusions/particles of various sizes are evaluated. The resulting plots are shown as Fig. 6. Curve S1 is the reference curve. The characteristic length of surface-charge-bearing nonconductive particle seems have little effect on model predictions when both conductive and nonconductive particles are present in the mixture (as observed from the overlap between S1C1P1 and S1C2P1). For conductive inclusions, a smaller characteristic length will shift the frequency dispersion of σ_{eff} and $\epsilon_{r,eff}$ response to higher frequencies (i.e. shift the curves towards right in both the plots). Therefore, σ_{eff} reduces and $\epsilon_{r,eff}$ increases for mixtures containing conductive particles of smaller characteristic lengths.

3.5. PS model sensitivity to the volume fractions of conductive and nonconductive spherical particles

The effects of volume fraction of nonconductive and conductive particles are evaluated in this section. Fig. 7 shows the result, where Curve S1 is the reference curve. Comparing S1C1P1, S1C2P1 and S1C1P2 curves in Fig. 7a, an increase in volume fraction of surface-charge-bearing nonconductive particles increases the magnitude of the frequency dispersion of σ_{eff} due to the increase in the net polarization ef-

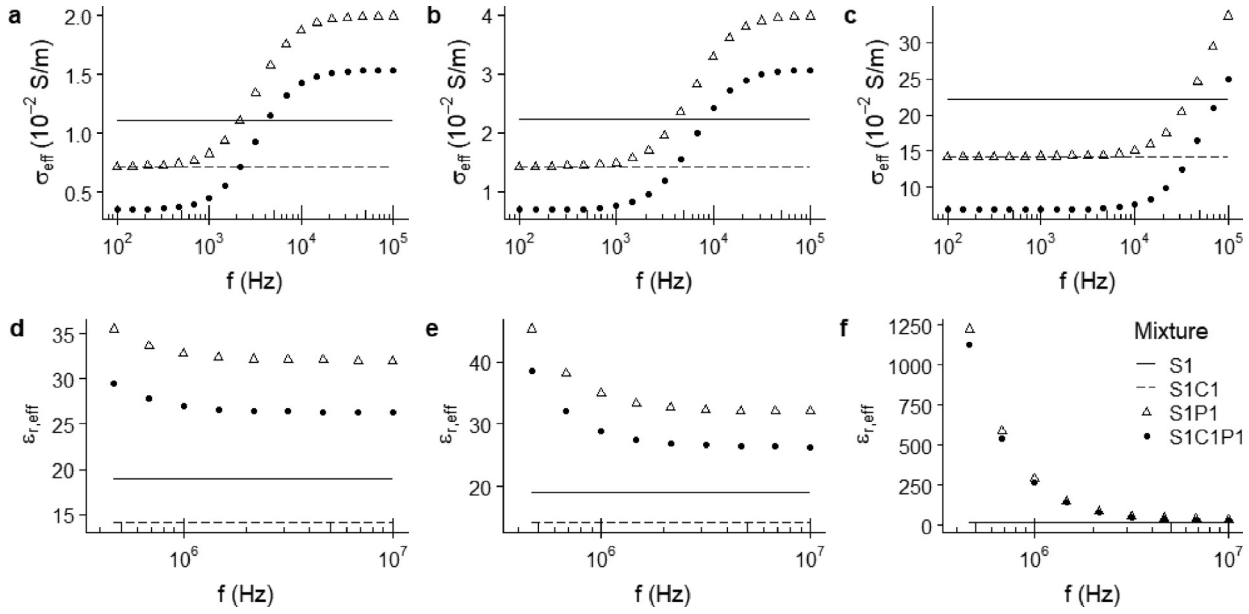

Fig. 8. Comparison of the PS model predictions of (a) σ_{eff} and (b) $\varepsilon_{r,eff}$ of mixtures containing spherical sand, clay and pyrite particles (properties listed in Table 6) and fully saturated with electrolyte of various conductivity σ_h, $\varepsilon_{r,h}$ of 70, and D_h of 10^{-9} m^2/s. (a), (b), (c) represent σ_{eff} prediction, and (d), (e), (f) represent $\varepsilon_{r,eff}$ prediction for mixtures fully saturated with 0.05, 0.1, and 1 S/m electrolyte, respectively.

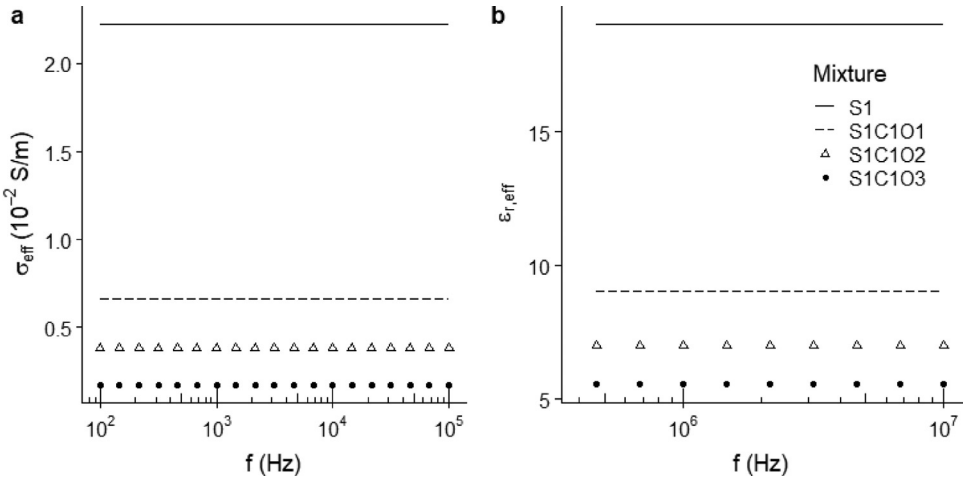

Fig. 9. Comparison of the PS model predictions of (a) σ_{eff} and (b) $\varepsilon_{r,eff}$ of mixtures containing spherical sand, clay and pyrite particles partially saturated with electrolyte of $\varepsilon_{r,h}$ of 70, σ_h of 0.1 S/m and D_h of 10^{-9} m^2/s and containing different volume fractions of oil. The properties of sand, clay, pyrite and oil are listed in Table 7. O1–O3 represent oil volume fractions of 1%, 5% and 8% (which correspond to oil saturation of 5%, 25% and 40%, respectively, if porosity is 20%).

Table 6
Properties used for generating Fig. 8, where S1 represents sand, C1 represents clay, and P1 represents pyrite and the host is an electrolyte of $\varepsilon_{r,h}$ of 70 and D_h of 10^{-9} m^2/s.

	ϕ_i (%)	a_i (μm)	D_i (m^2/s)	$\varepsilon_{r,i}$	σ_i (S/m)	λ (S)
Sand (S1)	70	1000	–	4	–	10^{-9}
Clay (C1)	10	100	–	8	–	10^{-8}
Pyrite (P1)	10	200	5×10^{-5}	12	500	–

fect; this appears as a downward shift. On the other hand, an increase in the volume fraction of conductive particles, causes a steep rise (a high rate of increase) in the frequency dispersion of σ_{eff}. For frequencies lower than 1 kHz, σ_{eff} values are constant. Comparison of S1C1P1, S1C2P1 and S1C1P2 curves in Fig. 7b indicates an increase in the volume fraction of nonconductive particles shifts the frequency dispersion curve of $\varepsilon_{r,eff}$ to lower values, while an increase in volume fraction of conductive particles shifts the curve to much larger values.

3.6. PS model sensitivity to the conductivity of pore-filling electrolyte

The effects of conductivity of electrolyte are evaluated in this section. As for σ_{eff} prediction, we can clearly observe that the increase of electrolyte conductivity shifts the dispersion to higher frequencies (right shift). The low-frequency dispersion can hardly be observed for electrolyte with conductivity value higher than 1 S/m (Fig. 8c). When the electrolyte conductivity is increased by one order of magnitude, the corresponding σ_{eff} prediction also increases by one order of magnitude, similar to Archie's law. As for $\varepsilon_{r,eff}$ prediction, it can also be concluded that $\varepsilon_{r,eff}$ is positively related to the conductivity of electrolyte because a greater charge carrier concentration in electrolyte leads to greater charge accumulation around the interface. Moreover, the conductive particles dominate the prediction of $\varepsilon_{r,eff}$ for frequencies below 5 MHz, especially with the conductivity of the electrolyte is high.

3.7. PS model sensitivity to volume fractions of oil

In this paper, we model oil as nonconductive spherical droplets of specific size (100 μm) uniformly distributed in the mixture, so the effect

Table 7
Properties used for generating Fig. 9, where S1 represents sand, C1 represents clay, and O1–O3 represent different volume fractions of oil. The host is an electrolyte of $\varepsilon_{r,h}$ of 70, σ_h of 0.1 S/m and D_h of 10^{-9} m^2/s.

	ϕ_i (%)	a_i (μm)	D_i (m^2/s)	$\varepsilon_{r,i}$	σ_i (S/m)	λ (S)
Sand (S1)	70	1000	–	4	–	10^{-9}
Clay (C1)	20	10	–	8	–	10^{-8}
Oil (O1~3)	1, 5, 8	100	–	2	–	10^{-30}

of increase in oil saturation can be seen as that of increase in the volume fraction of a nonconductive spherical particle with unique properties, as described in Table 7. Comparing the curves with reference curve S1, we conclude that the increase in volume fraction of oil will decrease the σ_{eff} and $\varepsilon_{r,eff}$.

4. Conclusions

We developed a mechanistic model of multi-frequency complex conductivity for a homogeneous porous media containing surface-charge-bearing non-conductive particles (e.g. clays and sand) and conductive mineral particles (e.g. pyrite) saturated with oil and brine. The model accounts for the interfacial polarization (IFP) effects due to the surface conductance of clays and that due to the conductive particles.

We studied the IFP effects of clays and conductive minerals on the effective conductivity (σ_{eff}) in the frequency range of 100 Hz to 100 kHz and on the effective permittivity ($\varepsilon_{r,eff}$) in the frequency range of 0.5 MHz to 1 GHz. A decrease in size or an increase in the surface conductance of surface-charge-bearing nonconductive particles, referred herein as clays, uniformly distributed in a porous homogeneous mixture leads to a slight decrease in the σ_{eff} and an increase in the $\varepsilon_{r,eff}$. The effects of clay particles with the same ratio of size to surface conductance and the same relative permittivity (ε_r) on the complex conductivity of the mixture are similar. In the frequency windows mentioned above, the frequency dispersion of complex conductivity due to the IFP effects for clays are negligible compared to conductive particles.

The presence of conductive particles increases the $\varepsilon_{r,eff}$ and decreases the σ_{eff} at lower frequencies. A higher relative permittivity or conductivity of conductive particles increases σ_{eff} and decreases $\varepsilon_{r,eff}$ of mixture, whereas a higher diffusion coefficient of conductive particles decreases σ_{eff} and increases $\varepsilon_{r,eff}$. The effects of conductive particles with the same ratio of particle conductivity to diffusion coefficient and the same ε_r or those with the same value of conductivity times permittivity and diffusion coefficient on the complex conductivity of the mixture are similar. For conductive inclusions, a smaller size shifts the frequency dispersion of σ_{eff} and $\varepsilon_{r,eff}$ response to higher frequencies. Therefore, σ_{eff} reduces and $\varepsilon_{r,eff}$ increases for mixtures containing conductive particles of smaller characteristic lengths. For the conductive particles studied in this paper, the frequency dispersion in σ_{eff} occurs for frequency between 1 and 100 kHz, whereas the dispersion in $\varepsilon_{r,eff}$ occurs for frequency lower than about 5 MHz.

An increase in volume fraction of surface-charge-bearing nonconductive particles increases the magnitude of the frequency dispersion of σ_{eff} due to the increase in the net polarization effect; this appears as a reduction in σ_{eff}. On the other hand, an increase in the volume fraction of conductive particles, causes a steep rise (a high rate of increase) in the frequency dispersion of σ_{eff}. An increase in the volume fraction of nonconductive particles shifts the frequency dispersion curve of $\varepsilon_{r,eff}$ to lower values, while an increase in volume fraction of conductive particles shifts the curve to much larger values. An increase in brine conductivity shifts the dispersion of σ_{eff} prediction to higher frequencies. When the brine conductivity is increased by one order of magnitude, the corresponding σ_{eff} prediction also increases by one order of magnitude, similar to Archie's law. The low-frequency dispersion can hardly be observed for electrolyte with conductivity value higher than 1 S/m. $\varepsilon_{r,eff}$ is positively related to the conductivity of electrolyte because a greater charge carrier concentration in electrolyte leads to greater charge accumulation around the interface. Moreover, the conductive particles dominate the prediction of $\varepsilon_{r,eff}$ for frequencies below 5 MHz, especially when the conductivity of the electrolyte is high.

Acknowledgments

We thank Dr. Chang-Tu Hou, senior scientist at Schlumberger-Doll Research Center, for valuable technical suggestions and for reviewing the paper before the publication. We thank Dr. Denis Heliot, Global Interpretation Métier Manager at Schlumberger, for his support that was very valuable during the initial stages of the project. Also, we thank Joe Zapf, Development Technician at Schlumberger, for handling logistics that streamlined the execution of this project.

Supplementary materials

Supplementary material associated with this article can be found, in the online version, at doi:10.1016/j.advwatres.2019.06.015.

References

Altman, R., Anderson, B., Rasmus, J., Lüling, M.G., 2008. Dielectric effects and resistivity dispersion on induction and propagation-resistivity logs in complex volcanic lithologies: a case study. In: Proceedings of the 49th Annual Logging Symposium. Society of Petrophysicists and Well-Log Analysts Jan 1.

Anderson, B.I., Barber, T.D., Lüling, M.G., Rasmus, J., Sen, P.N., Tabanou, J.R., Haugland, M., 2007. Observations of large dielectric effects on LWD propagation-resistivity logs. In: Proceedings of the 48th Annual Logging Symposium. Society of Petrophysicists and Well-Log Analysts Jan 1.

Chu, K.T., Bazant, M.Z., 2006. Nonlinear electrochemical relaxation around conductors. Phys. Rev. E 74 (1), 011501 Jul 6.

Clavier, C., Heim, A., Scala, C., 1976. Effect of pyrite on resistivity and other logging measurements. In: Proceedings of the SPWLA 17th Annual Logging Symposium. Society of Petrophysicists and Well-Log Analysts Jan 1.

Corley, B., Garcia, A., Maurer, H.M., Rabinovich, M.B., Zhou, Z., DuBois, P., Shaw Jr, N., 2010. Study of unusual responses from multiple resistivity tools in the Bossier formation of the Haynesville shale play. In: Proceedings of the SPE Annual Technical Conference and Exhibition. Society of Petroleum Engineers Jan 1.

Cosenza, P., Ghorbani, A., Camerlynck, C., Rejiba, F., Guérin, R., Tabbagh, A., 2009. Effective medium theories for modelling the relationships between electromagnetic properties and hydrological variables in geomaterials: a review. Near Surface Geophys. 7 (5–6), 563–578 Oct 1.

Deng, Y., Shi, X., Revil, A., Wu, J., Ghorbani, A., 2018. Complex conductivity of oil-contaminated clayey soils. J. Hydrol. (Amst) 561, 930–942 Jun 1.

Dukhin, S.S., Shilov, V.N., Bikerman, J.J., 1974. Dielectric phenomena and double layer in disperse systems and polyelectrolytes. J. Electrochem. Soc. 121 (4), 154C Apr 1.

Freed, D.E., Seleznev, N., Hou, C.Y., Fellah, K., Little, J., Dumy, G., Sen, P., 2018. A physics-based model for the dielectric response of shaly sands and continuous CEC logging. Petrophysics 59 (03), 354–372 Jun 1.

Garcia, A., Barchini, R., Grosse, C., 1985. The influence of diffusion on the permittivity of a suspension of spherical particles with insulating shells in an electrolyte. J. Phys. D Appl. Phys. 18 (9), 1891 Sep 14.

Giordano, S., 2003. Effective medium theory for dispersions of dielectric ellipsoids. J. Electrostat. 58 (1–2), 59–76 May 1.

Grosse, C., Barchini, R., 1992. The influence of diffusion on the dielectric properties of suspensions of conductive spherical particles in an electrolyte. J. Phys. D Appl. Phys. 25 (3), 508 Mar 14.

Grosse, C., 1988. Permittivity of a suspension of charged spherical particles in electrolyte solution. 2. Influence of the surface conductivity and asymmetry of the electrolyte on the low-and high-frequency relaxations. J. Phys. Chem. 92 (13), 3905–3910 Jun.

Grosse, C., Foster, K.R., 1987. Permittivity of a suspension of charged spherical particles in electrolyte solution. J. Phys. Chem. 91 (11), 3073–3076 May.

Grosse, C., Schwan, H.P., 1992. Cellular membrane potentials induced by alternating fields. Biophys. J. 63 (6), 1632–1642 Dec 1.

Grosse, C., Tirado, M., Pieper, W., Pottel, R., 1998. Broad frequency range study of the dielectric properties of suspensions of colloidal polystyrene particles in aqueous electrolyte solutions. J. Colloid Interface Sci. 205 (1), 26–41 Sep 1.

Hogg A.J. Fluid dynamics separable solutions to Laplace's equation. 2001. https://people.maths.bris.ac.uk/~maajh/fluids/handout3.pdf

Hou, C.Y., Feng, L., Seleznev, N., Freed, D.E., 2018. Low frequency complex dielectric (conductivity) response of dilute clay suspensions: modeling and experiments. J. Colloid Interface Sci. 525, 62–75 Sep 1.

Leroy, P., Revil, A., 2004. A triple-layer model of the surface electrochemical properties of clay minerals. J. Colloid Interface Sci. 270 (2), 371–380 Feb 15.

MacLennan, K., Karaoulis, M., Revil, A., 2013. Complex conductivity tomography using low-frequency crosswell electromagnetic data. Geophysics 79 (1), E23–E38 Nov 22.

Martinez, A., Brynes, A.P., 2001. Modeling Dielectric-constant Values of Geologic Materials: An Aid to Ground-penetrating Radar Data Collection and Interpretation. Kansas Geological Survey, Lawrence, KS Dec.

Misra, S., Torres-Verdín, C., Revil, A., Rasmus, J., Homan, D., 2016a. Interfacial polarization of disseminated conductive minerals in absence of redox-active species—Part 2: effective electrical conductivity and dielectric permittivityInterfacial polarization due to inclusions. Geophysics 81 (2), E159–E176 Mar 1.

Misra, S., Torres-Verdín, C., Revil, A., Rasmus, J., Homan, D., 2016b. Interfacial polarization of disseminated conductive minerals in absence of redox-active species—Part 1: mechanistic model and validation. Geophysics 81 (2), E139–E157 Mar 1.

Placencia-Gómez, E., Slater, L.D., 2014. Electrochemical spectral induced polarization modeling of artificial sulfide-sand mixtures. Geophysics 79 (6), EN91–E106 Sep 23.

Revil, A., 2013. Effective conductivity and permittivity of unsaturated porous materials in the frequency range 1 mHz–1 GHz. Water Resour. Res. 49 (1), 306–327 Jan.

Revil, A., 2012. Spectral induced polarization of shaly sands: influence of the electrical double layer. Water Resour. Res. 48 (2) Feb 1.

Revil, A., Murugesu, M., Prasad, M., Le Breton, M., 2017. Alteration of volcanic rocks: a new non-intrusive indicator based on induced polarization measurements. J. Volcanol. Geotherm. Res. 341, 351–362 Jul 15.

Revil, A., Abdel Aal, G.Z., Atekwana, E.A., Mao, D., Florsch, N., 2015. Induced polarization response of porous media with metallic particles—Part 2: comparison with a broad database of experimental data. Geophysics 80 (5), D539–D552 Aug 12.

Schmuck, M., Bazant, M.Z., 2015. Homogenization of the Poisson–Nernst–Planck equations for ion transport in charged porous media. SIAM J. Appl. Math. 75 (3), 1369–1401 Jun 30.

Schwarz, G., 1962. A theory of the low-frequency dielectric dispersion of colloidal particles in electrolyte solution1, 2. J. Phys. Chem. 66 (12), 2636–2642 Dec.

Sihvola, A., 2007. Dielectric polarization and particle shape effects. J. Nanomater. 2007 (1), 5.

Tuncer, E., Gubański, S.M., Nettelblad, B., 2001. Dielectric relaxation in dielectric mixtures: application of the finite element method and its comparison with dielectric mixture formulas. J. Appl. Phys. 89 (12), 8092–8100 Jun 15.

Weisstein E.W. Legendre polynomial. http://mathworld.wolfram.com/LegendrePolynomial.html; 2018a, accessed 11 Nov 2018.

Weisstein E.W. Bessel function. http://mathworld.wolfram.com/BesselFunction.html; 2018b, accessed 11 Nov 2018.

Wong, J., 1979. An electrochemical model of the induced-polarization phenomenon in disseminated sulfide ores. Geophysics 44 (7), 1245–1265 Jul.

Young, P., 2009. Helmholtz's and Laplace's Equations in Spherical Polar Coordinates: Spherical Harmonics and Spherical Bessel Functions. University of California, Santa Cruz, CA, p. 116. Physics 116C Lecture Notes http://physics.ucsc.edu/~peter.

Zhao, P., Zhuang, W., Sun, Z., Wang, Z., Luo, X., Mao, Z., Tong, Z., 2016. Methods for estimating petrophysical parameters from well logs in tight oil reservoirs: a case study. J. Geophys. Eng. 13 (1), 78–85 Jan 29.

Zheng, Q., Wei, G.W., 2011. Poisson–Boltzmann–Nernst–Planck model. J. Chem. Phys. 134 (19), 194101 May 21.